Evaluation of the organization of the homoionic smectite layers (Na+ or Ca2+) in diluted dispersions using granulometry, microscopy and rheometry

S. Paumier, A. Pantet, P. Monnet

Evaluation of the organization of the homoionic smectites layers (Na^+ or Ca^{2+}) in diluted dispersions using granulometry, microscopy and rheometry.

S. PAUMIER [a,b], A. PANTET[b], P. MONNET [b]

[a]Hydrologie Argile Sol et Altération[b] CNRS, University of Poitiers, 40 avenue du recteur Pineau, 86022 Poitiers. France.

[b] Laboratoire d'Etudes Aérodynamiques (LEA), ENSMA, CNRS, University of Poitiers, 40 avenue du recteur Pineau, 86022 Poitiers. France.

Sandrine PAUMIER

Phone: +33 1 40 96 62 14

Fax: +33 1 40 96 60 36

E-mail of the corresponding author: sandrine.paumier@cemagref.fr

ABSTRACT

Smectites are swelling clay materials with pronounced colloidal properties that are widely used in industry. These properties originate in the electrokinetic properties of the smectite layers and their linkage capacities. Thin layers may be dispersed or aggregated according to many parameters, such as concentration, particle size and morphology, exchangeable cation nature and chemical environment (pH, ionic strength). The literature usually provides general rules, like the sodium dispersion contains a lot of small units whereas the calcium dispersion contains a few large units. A volume of water molecules bound to the clay surface is considered as the immobile water phase that behaves like the solid phase obstructing the flow. The water immobilized around layers and trapped inside aggregates can not participate to the flow.

In this study, we evaluated the volume occupied by calcium and sodium units inside the dispersion containing the immobile water phase. First, the smectite was cautiously extracted from a raw bentonite and its physicochemical properties were determined. A large quantity of extracted and saturated smectite (Na-smectite and Ca-smectite) was obtained. Second, the unit size and a shape

factor for each sample were evaluated using granulometry and scanning transmission electron microscopy on wet samples (Wet STEM) and some flow curves. Na-smectite dispersions contain 0.13µm² surface units with a shape factor of 50. Ca-smectite dispersions contain 0.32 µm² surface units with a shape factor of 3.3. Finally, rheometry allowed us to evaluate the unit occupancy using an adaptation of the Krieger- Dougherty law. We used shape factors and evaluated the concentration from which the entire immobile volume was connected (6.4% for Na-smectite and 11.9% for Ca-smectite).

This study explains the evolution of flow properties with increasing concentrations by the evolution of layer interactions at the microscopic scale for homoionic smectite particles in diluted dispersions.

INTRODUCTION

The smectite contents in bentonites provide viscoelastic and adsorption properties that are widely used in industries [1] [2] like the construction [3] and the chemical [4] [5] industries, as well as in the environmental survey [6]. These properties originate in the swelling capacities of smectite layers. In water, smectite units form colloidal dispersions and may develop a complex network depending on the concentration, the unit size, the exchangeable cation nature and the physicochemical properties of the suspending fluid. The swelling capacity of a bentonite is generally attributed to the volume of water molecules that is bounded to the clay surface. These water molecules are considered as the immobile phase that behaves like the solid phase obstructing the flow. As the volume of bound water molecules increases and the immobile water phase thickens, the effective pore space comprised of freely flowing water decreases. At the macro-scale, an increase in the bound water means an increase in the mechanical properties (viscosity, yield stress, thixotropy). The volume of bound water has traditionally been described in the electric diffusion double layer using the DLVO theory [7] [8] [9]. However, the DLVO theory does not describe the crystal interlayer expansion and the water entrapped in the case of layer association [10] [11].

Many parameters can modify the smectite layer association: the properties of the smectite sheets (mineralogy, size, structural charge, exchangeable cations…) [12] [13] [14 [15] [16] [17] [18] [19], the ionic environment [20] [21] [22] [23] [24] [25] [26], the solid/liquid ratio [20] [27], the solution chemistry [28], the organic matter [29], and the dispersion preparation.

We focused on the impact of the exchangeable cation (calcium or sodium) and the solid/liquid ratio because their effects were verified for a lot of smectites. The main well-known rule states that the exchangeable cation effect results in contrasted modes of layer linkage. Smectite layers are aggregated into tactoïds in the case of calcium-saturated dispersions and are delaminated in the case of sodium-saturated dispersions [30] [31] [32]. Under shear rate, these two arrangements result in contrasted mechanical properties that can be characterized with a rheometer.

The bibliography provides many rheological studies on bentonites, the aims and methods of which greatly vary. Many authors described the rheological properties of complex fluids (thixotropy [33] [34] [35], yield stress [36] [37] [38] [39], visco-elasticity [40] [41]) and how to characterize them). Other authors studied the heterogeneities generated inside the geometry of the rheometer when complex fluids were used [42] [43]. These authors were generally not interested in the bentonite composition, but rather in their mechanical properties. Several authors reported on the colloidal state of the dispersion [28] [44]. They used flow curves as a characterization tool to determine two comparison parameters: the plastic viscosity and the apparent yield stress using the Bingham law (Eq. (1)). In most cases, however, the flow curves clearly show the shear-thinning behavior of the smectite dispersions, and the Ostwald law (Eq. (2)) or the Herschel Bulkley law (Eq. (3)) is to be preferred. In this case, rheology was used to obtain comparison values.

Bingham's model: $\tau = \tau_P + \eta_B \dot{\gamma}$ (1)

Ostwald's model: $\tau = k \dot{\gamma}^n$ (2)

Herschel Bulkley's model: $\tau = \tau_0 + k \dot{\gamma}^n$ (3)

where τ (Pa) is the shear stress, $\dot{\gamma}$ (s^{-1}) is the shear rate, τ_P (Pa) is the plastic yield stress, η_B (Pa.s) is the Bingham viscosity, k ($Pa.s^n$) is the consistency, n is a phenomenological coefficient and τ_o (Pa) is the yield stress.

Keren [17] [20] took into account the shear-thinning behavior of fluids; he characterized the smectite in various saturation states with flow curves. Similarly, our study dealt with extracted and saturated samples at low concentrations (Newtonian or shear-thinning behavior without yield stress). We provided other preparation processes because Keren's processes were not efficient on our material. We elaborated on this issue by using rheometry to evaluate a maximum volume fraction of the solid dispersed at rest (ϕ_m). The model, usually used on spherical balls, was adapted to the clay particle anisotropy using a shape factor. We used microscopic and granulometric measurements and bibliographic data to evaluate these factors (Simha's factors).

In the first part, we successively described the physicochemical solid/water interactions, the preparation processes and the dispersion preparation (mixing power, hydration time, etc.). The stocks were accurately described in terms of mineralogy and physicochemical properties. They will be used in several projects in order to gradually complicate the system. In the second part, we studied the unit size for each sample by laser granulometry and we observed the particles inside the dispersion in the diluted state (less than 3 %). These results allowed determining a shape factor to account for the high anisotropy of the clay units. The Krieger-Dougherty law was applied to the rheological results in order to assess the solid volume fraction, i.e. the fraction of the total volume occupied by solid particles.

In brief, each scientist community has its own tools, and authors usually work on mineralogy or rheology with poor interactions. Rheometry can be used not only to determine the yield stress and thixotropic behavior, but also to evaluate the volume occupied by clay particles in dispersion. Our issue was to establish the relationship between the characteristic factors of smectite units and their mechanical response under shear rate. We had to connect the mineralogical,

morphological and mechanical properties from the study of diluted then concentrated dispersions, first for homoionic dispersions, then for bi-ionic dispersions. In this study, we focused on the unit characterization (size and connectivity) of homoionic smectite dispersions at low concentrations.

MATERIAL AND METHODS

A large amount of smectite estimated at 800 g was necessary to apply a large variety of methods, including a complete rheological program with all the repeatability and reproducibility requirements. The treatment of a raw bentonite in order to extract and saturate the fine fraction was cautiously monitored at each step using physicochemical tests. It allowed to verify the process efficiency and to detect the process, thus optimizing both quality and quantity. The preparation of the material required the use of several methods, so we chose to present in a first part the methods then the material and it preparation.

We studied Na-smectite and Ca-smectite in various states from the dry powder to the diluted dispersion. X-Ray diffractometry (XRD), differential thermal analysis (DTA) and laser granulometry were used to verify the smectite homogeneity (no additive nor accessory mineral) and to analyze the powder properties (unit size and hydration). Microscopic observations were difficult due to dispersion opaqueness and layer flexibility. Various methods have been developed to fix dispersions by inclusion, cryonic or freeze-drying but they still lead to artifacts [45] [46]. In this study we observed clay units in dispersion using cutting-edge technology, named Wet STEM (scanning transmission electron microscopy on wet samples). Rheological measurements and swelling index gave information on the shear strength of the dispersion indicating the interaction intensity between the units. The Krieger-Dougherty law allowed the evaluation of the solid volume fraction. It was adapted to clay minerals using a shape factor in order to account for the high anisotropy of clay units.

1. X-Ray diffraction

The clay mineralogy was analyzed by X-ray diffraction (XRD) (Philips X'Pert PRO PW3050/6x goniometer using Fe-filtered CuKα radiation, 40 kV, 40 mA). Randomly-oriented

powders were analyzed in the 2-65 ° 2θ range with a step of 0.05 ° 2θ (3 s per step). Sherrer's equations gave the crystalline index [47]. Oriented preparations were prepared by sedimentation of the dispersion (in average 0.05 %) then drying under hood. The oriented preparations were analyzed in the 2 - 35 ° 2θ range with a step of 0.025 ° 2θ (4 s per step) in the natural state and saturated with ethylene glycol (12-hour contact under vacuum).

2. DTA

Differential thermal analysis (NETZSCH Simultan STA 409 EP analyzer, DTA) was performed with a heating rate of 10 °C per minute over the 20 °C - 1100 °C temperature range. DTA ensured the natural state of the fine fraction and tested the cation hydration.

3. Granulometry

The granulometry of the sixteen samples was measured with a Malvern Metasizer IP granulometer (45 mm focal length lens) after complete disintegration. The powder (0.1 g) was dispersed in osmosed water (200 ml) with 1 ml of sodium hexamethaphosphate (10.2 %) and sonified for 1 min (20 kHz, Bioblock vibra-cell 75041). The measurement was linked to the dispersion opaqueness so the concentration could not be set exactly (almost 0.05 %).

4. Chemical analysis

Carbonate and organic matter contents were measured using the Bernard calcimeter (Prolabo 05 215,00) and the Walkley-Black titrimetric processes on the raw bentonite. The fluid surrounding the material in the dispersion state was characterized after filtration under pressure (700 kPa) using an API filter press RP13I equipped with a cylindrical cell of 90 mm in diameter and 90 mm in height. Anionic and cationic contents from the filtrate were analyzed using an Ion Chromatography System (ICS 1000) and Flame Atomic Adsorption Spectroscopy (Perkin Elmer 3110, FAAS). Raw bentonite dispersions (30 % in mass concentration) were filtered for one hour with the filter press. Four hydration periods were tested between the preparation time and the beginning of the filtration (0 hour, 3 hours, one day, one month and 3 months). No acidic treatment

was used to avoid changes in clay properties. The use of heat and ultrasonic treatments were reduced as much as possible.

The conductivity was measured with a Consort k810 conductimeter standardized with a buffer solution at 1413 µS.cm^{-1}. The pH was measured with a Metrohm Heris E 250 pH-meter standardized with buffer solutions at pH 7 and pH 10.

The CEC and exchangeable cations were measured using the ammonium method. The material was first saturated with ammonium: 100 mg of powder material was dried at 105 °C and brought into contact with 1 *M* NH_4Cl solution (pH = 7) five times for one hour. The supernatants were collected and analyzed by FAAS. The remaining material was washed with ethanol in order to remove the excess ammonium and the CEC was determined after Kjeldhal distillation (AFNOR standard X 31,130 Nov 1985).

5. Wet STEM

The Wet STEM observation method implies the use of an environmental scanning electron microscope (ESEM). The ESEM enables wet samples to be observed without potentially damaging sample preparation through the use of partial water vapor pressure in the microscope specimen chamber. In the Wet STEM method, a special device, developed by Bogner *et al.* [48], allows observation of an object submerged in a liquid under annular dark-field imaging conditions. A droplet of dispersion aged for one week was highly diluted (0.01 %) and dropped on the grid with an eppendorf micropipette. The Na-smectite dispersion needed higher dilution (0.001 %) to meet clarity requirements. Under these conditions, the incident electron beam passed through the droplet, i.e. the liquid layer and a given amount of floating units. The signal was then collected by a detector, typically used for the collection of backscattered electrons (BSE), but in our case located below the sample. We used holey carbon-coated TEM copper grids, with the carbon layer down, in order to use copper squares as retention basins. In the carbon layer, holes of typical diameter ranging from less than 1 µm to 20 µm enabled the liquid films to be confined within very small spaces. Units of each view were approximated to ellipses by image processing using the Nikon

Imaging Software (NIS). The ellipse areas were plotted against the observation frequency in order to draw a frequency curve.

6. Swelling tests

Swelling tests were performed before rheological tests in order to analyze the hydration capacities of each sample. The powder (0.2 g) was gradually added to osmosed water (10 ml) in a borosilicate cylinder. The swelling was read after 24 h of hydration.

6. Rheology

The rheological methods are sensitive enough to quantify very accurate variations in the micro-structure [49] [50] [51]. The rheometer gives an average value of all the shear rates produced between the plates [52]. The rheological measurements were performed with a Gemini HR stress-controlled rheometer (Malvern Instrument). Many dispersions were prepared at 0.2 % to 4 % (w/w) using the reference process. Experimental flow curves were obtained with rough parallel-plate geometry (40 mm) spaced 500 µm apart. A preshear at 100 s^{-1} was imposed for 60 s followed by a rest period of 180 s before each test in order to put the dispersions in an initial structural state. Then, the dispersions were subjected to increasing and decreasing shear rates for 30 min by 60 steps from 0.001 s^{-1} to 500 s^{-1}. When data from this test are plotted in a graph, the area between the increasing and decreasing curves defines the thixotropic area. When the dispersion stability was low (for concentrations inferior to 4 %), the rest period was reduced to 5 s, then the dispersions were subjected to increasing and decreasing shear rates for 7 min by 20 steps from 0.1 s^{-1} to only 150 s^{-1} in order to avoid the occurrence of vortex due to the low viscosity. The stability of dispersions against sedimentation was verified by agreement of successive tests.

8. Fractionation and cation saturation

The raw bentonite was received as decimetric blocks from Sardinia (BENTO France Company). Several heterogeneous blocks were broken apart before bentonite quartering (Terratest – Soiltest inc). The bentonite (200 g) was dispersed in osmosed water (500 ml, pH= 6.5 and

conductivity 5 µS.cm^{-1}) and sieved at 80 µm using a strainer and addition of osmosed water (500 ml). The filtrate (one liter) was let at rest in an air-conditioned room (20 °C). The total hydration time was 36 hours, during which the soluble salts were dissolved and the thermal equilibrium was reached.

A standard centrifugation method [20] [44] consists in collecting the supernatant after successive centrifugation-dilution cycles. In order to optimize the extraction process, we isolated each collected sample and studied them with laser granulometry and XRD measurements up to the sixteenth cycle. The supernatants after each centrifugation (Jouan GR 422) at 1,000 rpm for 161 s were collected, and then isolated in an evaporating dish made of glazed porcelain. The centrifugation pellet was mixed with clear osmosed water (200 ml, 20°C) and another cycle was run. At each cycle, the conductivity and pH were measured. Each suspension was dried in an evaporator at 70 °C. The dried material was cautiously removed from the evaporating dish and weighted in a tare vessel. The sixteen samples were lightly crushed with agate pestle and mortar (*ff-1* to *ff-16).* These drying and crushing steps allowed aliquot homogenization.

The successive dilutions induced the drop in conductivity from 142 µS after the first cycle to approximately 5 µS after the 11th cycle. Then the conductivity remained stable. The sample pH was stable at 9.5 up to the 8th cycle, and then the pH decreased strongly. The mass of dried material extracted at each cycle dropped quickly between the first cycle (7 g) and the fourth cycle (2 g), and then the mass stabilized at 1.2 g of clay per cycle.

The X-ray diffractograms of the 1st, 4th, 8th and 12th oriented preparations are shown in Figure 1. The main peak corresponds to the d_{001} reflection peak of smectite. Accessory minerals as quartz (3.35 Å) and feldspars (3.22 Å) were detected in each cycle.

Figure 1

Laser granulometry curves showed that the extracted fraction was markedly above 2 µm after the 8^{th} cycle (Figure 2). As a result, the process had to be stopped at the seventh step. Consequently, with seven extraction cycles, we extracted 10 g of fine fraction from 100 g of bentonite. This process was repeated eighty times, and the resulting materials were mixed, dried (evaporator Jouan 774 G 7) and crushed for 1 min in a vibrating cup mill (Sodomi CB 2200, 50 Hz), yielding 800 g of homogenized smectite in five weeks.

Figure 2

9. Calcium- and sodium-exchanged smectite

A standard exchange process consists in contacting the clay with a salted solution, like NaCl or $CaCl_2$, during five one-hour periods [20] [44]. However, the process efficiency may vary according to the clay properties [19] [22]. The saturation rates (reported in Table 1) were deduced from the ammonium exchange and FAAS measurements. The standard method was not appropriate for saturating our fine fraction, whether for calcium saturation (84.5 $meq.l^{-1}$ represent 85 % of the sum of the exchangeable cations) or for sodium saturation (30 %). Various factors were tested in order to enhance the saturating method. First, the dispersion was shaken over the whole contact time to prevent the powder from depositing. Then, the impact of contact time, concentration of the saturating solution, solid/liquid ratio, shaking energy and shaking time on clay saturation was tested. Successive L8 experimental designs described by Fisher [53] and Taguchi [54] were applied in order to specify the best level of each parameter. It appeared that the main parameters were the high concentration of the saturating solution and the high solid/liquid ratio. The contact time had also a great impact on the saturation efficiency, especially for Na-smectite. It could be related to the hydration time of the clay layers.

Table 1

Finally, the Ca-smectite powder was obtained by successive contacts (four 2-hour periods and one 12-hour period) between the dried fine fraction and a calcium chloride solution (1 *N* $CaCl_2$) at 15 % w/w. Centrifugations (17,000 rpm for 15 min) were performed between each contact period. For sodium saturation, the dried fine fraction was put in solution with 2 *N* NaCl (about 15 % w/w) and stirred five times for 12 h. After this saturation treatment, Ca-smectite and Na-smectite were dialyzed against osmosed water until the solution was free of chloride as indicated by the $AgNO_3$ test. The salt-free material was dried (60 °C) and mechanically crushed with a vibrating cup mill (1 min). Powders were stored at 20 °C in a desiccator over P_2O_5. The CEC and the exchangeable cations of Na-smectite and Ca-smectite were evaluated to test the efficiency of the saturation process. The whole stocks were processed at the same time, with the same method and an accurate control of the hydration times.

10. Dispersion preparation processes

Three preparation processes corresponding to three objectives were used:

- the *hydration process* allowed determination of granulometry after a 24-h hydration period (including 10 mixing hours at 50 rpm, Prolabo rotating shaker) without any mechanical or chemical disintegration treatment. This process reflected the natural state of smectite in dispersion.
- The *reference process* included the hydration process plus 1 min of mixing at 11,000 rpm with a homogenizer (IKA Ultra-Turrax T25). The mixing increased the disintegration without modifying the smectite saturation.
- The *standard process* included the hydration process plus the addition of 1.1 ml of sodium hexamethaphosphate (10.2 %) to the dispersion and the application of a 1-min ultrasonic treatment. This process allowed measurement of the elementary units.

The dispersions after the use of the three preparation processes were tested by laser granulometry. The *reference process* was also used for microscopic observations and rheometric tests.

The shaking time and shaking energy were cautiously checked during the dispersion preparation in order to ensure reproducibility and to allow comparisons of the rheological tests. The equilibrium pH of 8.4 ± 0.1 was not modified. For a better understanding, the dispersion was defined as "a two-phase system with interactive (attractive) colloidal solid units in a low molecular liquid system" as stated by Coussot and Van Damme [55]. According to Pawlick [56] and Peysson [57], "the dispersion is stable if the mean unit size distribution is stationary in time and space over a rest period longer than the testing period".

RESULTS

In this part, we present the successive results obtained from the raw bentonite to the two saturated powders in the dried and the diluted states.

1. From raw bentonite to saturated samples.

The sieving of the raw material in water revealed a significant part of coarse and intermediary materials (12 % of > 200 µm fractions and 42 % of fractions from 2 µm to 200 µm), with the fine fraction (< 2 µm) representing only 46 %. Neither carbonate nor organic matter contents were detected. The mineralogical study (XRD and optical microscopy) displayed a well-crystallized smectite (bold values) and some accessory minerals (Figure 3) such as quartz (4.260 Å, 3.350 Å), anorthite (3.224 Å, 1.542 Å), opal CT (4.069 Å), mica (3.651 Å), and magnetite (2.520 Å).

Figure 3

Hydration of the raw bentonite with osmosed water led to a quick ion release (Table 2). After one hour of test, without preliminary hydration delay, the conductivity reached 317 µS. The main ions existing in the solution were chloride (Cl^-), sodium (Na^+) and sulphate (SO_4^{2-}) (Table 2). The bentonite may contain some soluble sodium salts such as sodium chloride (*NaCl*) and sodium

sulphate (Na_2SO_4). Sodium carbonate (Na_2CO_3) and sodium bicarbonate ($HNaCO_3$) may form by atmosphere equilibrating. Ion concentrations increased during the first hydration day, then reached a relative equilibrium. Therefore, the concentration values after one month were a little bit higher.

Table 2

A comparison between the raw bentonite and the fine fraction in XRD diagrams confirmed the efficiency of the separation process (Figure 3). The d_{060} reflection peak at 1.50 Å pointed to a dioctahedral smectite. Oriented preparations were saturated with ethylene glycol. In this case, the d_{001} reflection peak shifted from 15.02 Å to 17.18 Å. The SEM/EDS analysis gave percent oxide contents presented in Table 3. The calculated structural formula revealed a few tetrahedral substitutions and more octahedral substitutions resulting in a charge deficit per unit cell of 0.550 compensated by Na^+, Ca^{2+}, Mg^{2+} and K^+ in the exchangeable complex.

Table 3

The exchangeable complex of the clay contains 49.5 % Ca^{2+}, 29 % Mg^{2+}, 19.5 % Na^+, and 2 % K^+, according to the ammonium method (Table 1). The comparison between the fine fraction and the two resulting samples (Ca-smectite and Na-smectite) argued for the good efficiency of the optimized saturation process (94 %) in relation to the standard process. Magnesium and potassium contents could not be reduced to less than 6 %; however, their concentrations seemed to remain unchanged in the exchangeable complex.

2. Comparative tests on Ca-smectite and Na-smectite

The influence of the exchangeable complex on the smectite unit morphology was monitored in various hydration states and various solid/liquid ratios.

2.1. Hydration state and mineralogical content (DTA and XRD)

DTA analyses were performed on each saturated sample. All peaks matched with a smectite powder [58]. Data showed a large low-temperature endothermic peak system (whose size, shape and temperature depend on the saturating cation), a medium-small endothermic peak at 648 °C and a small endothermic peak at 850 °C. These peaks were due to loss of sorbed moisture, mostly interlayer, dehydroxylation, and structural changes, respectively. DTA of the Ca-smectite powder displayed two separated peaks at 100 °C and 172 °C (Figure 4), corresponding to a weight loss of 9.7 % and 5.5 %, respectively. DTA of the Na-smectite powder displayed only one peak at 92 °C, i.e. 4.3 % of weight loss. These differences resulted from the high hydration energy of Ca^{2+} leading to the formation of two distinguished water layers between units. In contrast, Na-smectite contained a single short-developed water layer [58].

Figure 4

The occurrence of two water layers between the clay layers for the Ca-smectite powders led to a gap measured with XRD (Figure 5). Bragg's law was applied to the d_{001} reflection peak for each sample. The interlayer spacing was 15.02 Å for Ca-smectite and only 12.59 Å for Na-smectite. According to the Scherrer equations [47], the Na-smectite units were larger (B = 211 Å) and contained more layers (N = 17) than the Ca-smectite units (B = 186 Å and N = 12) in the dried state under ambient conditions.

Figure 5

2.2. Unit size by laser granulometry

The units were measured after three contrasted preparation processes to evaluate the layer aggregation (Figure 6a). The granulometric curves (Figure 6b) of the Na-smectite powders after the

hydration process outlined a high disintegration into small units. The distribution was bimodal with the first mode at 0.6 µm and the second at 2.1 µm. The index of the curves were d_{10} = 0.3 µm, d_{90}= 3 µm, and d_{50}=1 µm (Figure 6e). The Ca-smectite dispersion was monomodal (5.3 µm mode) but the distribution was dispersed: d_{10}=1.9 µm, d_{50}=7.2 µm and d_{90}=51.8 µm. We recalled, in accordance with Mie's theory assuming spherical-shaped units, that the d_{50} value means that fifty percent of the unit volume is composed of less than 1 µm-diameter units for Na-smectite and less than 7.2 µm-diameter units for Ca-smectite.

Figure 6

After the standard process, the modes of the Ca-smectite curve were the same as the Na-smectite curve but with a narrow shift of the relative values (Figure 6d). These results demonstrated that the initial granulometry of each sample was identical even after the mechanical crushing of the powder; the unit size was only related to the exchangeable complex. The Na-smectite unit sizes and the Ca-smectite elementary unit sizes were identical. The reference process confirmed the stability of the Na-smectite unit size in dispersion (Figure 6c). The Ca-smectite units showed a size intermediate between that from the two other preparation processes.

The disintegration treatment applied to the Na-smectite units did not enable modification of the granulometric curve. The material was in the most deflocculated state even after a mere hydration. In comparison, the Ca-smectite curve differed depending on the preparation treatment, the Ca-smectite units being formed from associated elementary units.

2.3. Unit size by Wet STEM

Each sample was observed by Wet STEM, and 10 photographs of each sample were analyzed with the NIS software. Each unit was assimilated to an ellipse of measurable area. Five hundred measurements were performed on the Na-smectite photographs and 150 measurements on the Ca-smectite photographs.

The Na-smectite units seemed to be placed side by side, and filled all the available space (Figure 7b). This observation could result from the three-dimensional superimposition or from the units settling down in the droplet. Unit sizes were quite homogeneous with a mean area of 0.13 µm². Unit distribution ranged from 0.03 µm² (d_{10}) to 0.31 µm² (d_{90}), however a few massive units were observed (Figure 7c).

The Ca-smectite unit sizes varied from 0.07 µm² (d_{10}) to 0.77 µm² (d_{90}), and were highly dispersed (Figure 7c). The units were dense and seemed to be composed of linked entities (Figure 7a). The small units were closed to the aggregates; they could result from the aggregate break-up probably due to the preparation process. Large spaces were occupied by water only.

Cadene *et al.* [59] studied MX-80 sodium montmorillonite with atomic force microscopy (AFM) and photo-correlation spectroscopy (PCS). Both techniques exhibited the presence of two clay populations with a high dispersion of the length distribution. The first population was typically 320–400 nm long/250 nm wide. The second population exhibited smaller sizes: 65 and 50 nm long. The particle surface of each population was 0,251-0,314 µm² and 0,007 µm², similar to our results.

Comparisons of the granulometric curves pointed out that the surface areas of the Ca-smectite units were 2.5 times larger than those of the Na-smectite units.

Figure 7

2.4. Swelling tests

The Na-smectite powder in water swelled quickly. After one hour, the volume occupied by the powder reached 80 % of the day's swelling. The sodium saturation led to a high swelling (4 cm^3) whereas the calcium saturation led to a small one (1 cm^3). These results were in accordance with those obtained by Besq *et al.* [60] on sixteen bentonites.

2.5. Rheological comparison tests

The mechanical behavior of the clay dispersion varied with concentration and type of clay. At low mass concentrations, the viscosity did not depend on the shear rate, and the fluid was Newtonian (Eq. (4)). This implied that the units flowed in water without contact nor interaction. The Na-smectite and Ca-smectite dispersions had a Newtonian behavior at concentrations below 4 % and 3 %, respectively (Figure 8, Table 4).

Newton's model : $\tau = \eta \dot{\gamma}$ (4)

where η (Pa.s) is the Newtonian viscosity.

Table 4

At higher concentrations, the viscosity decreased with the increasing shear rate, the fluid being of the shear-thinning type (Eq. (2), Table. 4). The shear-thinning behavior could originate in three phenomena: the orientation of the particles, the deformation of big entities and their crumbling. The break up of the entities led also to a thixotropic behavior of the dispersion.

Figure 8

For shear-thinning dispersions, we determined the relative viscosity at zero shear rate (η^*_0). The relative viscosity (η^*) refers to η/η_w where η_w is the viscosity of the dispersing medium (water), for Newtonian dispersions: $\eta^*_0=\eta^*$. Some models relate the volume fraction (ϕ) and the concentration (C). Among others is the well-known Einstein relationship (Eq. (5)):

Einstein's relationship: $\eta^* = 1 + \kappa\phi$ *(5)*

where κ is a shape factor, which varies with particle ellipticity.

The volume fraction (ϕ) of clay particles could not be easily calculated due to the material swelling. ϕ was the volume occupied by the hydrated units in dispersion. It included the volume

occupied by the layers surrounded by their diffuse double layers and the water entrapped inside the big entities. In our study, ϕ corresponded to the hydrated volume fraction of the entities.

In the Na-smectite dispersions, the units dispersed in water had a high extension and a low thickness. Güven and Pallastro [27] showed that κ ranged from 30 to 70 for flat particles with an ellipticity ratio (ψ) ranging from 50 to 100. In accordance with our results, we chose an intermediate value of $\kappa = 50$ for the Na-smectite dispersions.

The Ca-smectite dispersions contained big entities, and the Wet STEM results showed that their ellipticity ratio (ψ) was 2 to 3. According to the Kuhn and Kuhn relationship [61] (Eq. (6)), κ ranged from 2.9 to 3.7. We chose an intermediate value of $\kappa = 3.3$ for the Ca-smectite dispersions.

Kuhn and Kuhn's relationship: $$\kappa = \frac{3}{2}\left[\frac{\psi^2}{\psi^2 - 1}\right]\left[\frac{2\psi^2 - 1}{\psi\sqrt{\psi^2 - 1}}\ln\left(\psi + \sqrt{\psi^2 - 1}\right)\right] \quad (6)$$

where ψ is the ellipticity ratio.

The relative viscosities (η^*) of each sample were calculated and were reported against concentration in Figure 9. The curves suggested the use of the Krieger-Dougherty law (Eq. (7)).

Krieger Dougherty's law: $$\eta^* = \left(1 - \frac{\phi}{\phi_m}\right)^{-\alpha} \quad (7)$$

where ϕ_m is the maximum volume fraction of the solid dispersed, and α is usually equal to 2 [62].

Figure 9

By fitting our experimental curves, ϕ_m was equal to 0.61 for Ca-smectite and to 0.04 for Na-smectite. ϕ_m slightly differed from the usual definition, as it was not the maximal particle stacking inside the dispersion. ϕ_m was the solid fraction necessary to connect the total volume without hydrodynamic strength. The hydrated clay particles were arranged relative to each other in the dispersion and filled the total volume despite their low mass concentration. When ϕ_m was reached,

the concentration was named C_m. In the case of clay materials, it was possible to increase the solid fraction beyond C_m through mechanical stress.

For each species, ϕ was proportional to the mass concentration C ($\phi = fC$). The proportionality factor f depended on the swelling, the layer association and the water entrapped inside the entity. If C_m is the concentration associated to ϕ_m, then the Krieger Dougherty law is equal to :

$$\eta^{*-\frac{1}{2}} = 1 - \frac{C}{C_m} \quad (8)$$

We could determine C_m by fitting $\eta^{*-\frac{1}{2}}$ according to C (Figure 10). C_m was 6.4 % for Na-smectite and 11.9 % for Ca-smectite. These results corresponded to the detection of a yield stress in the dispersion (Table. 4).

Figure 10

DISCUSSION

This study clearly showed that the Na-smectite dispersions were composed of thin units (0.13 µm² equivalent ellipsoid surface) highly dispersed inside the dispersion (Wet STEM). The Na-smectite units could be disrupted neither by chemical treatment nor by agitation (laser granulometry). At concentrations below 3 %, the dispersions were of the Newtonian type. With our pH conditions (pH =8.4), these results were in accordance with other studies. The Na-montmorillonite dispersions were Newtonian at 1 % according to Janek and Lagaly [44], at 1 % to 4% for Kislenko and Verlinskaya [63], at 2.5 % for Keren [17] and Lagaly *et al.* [5]. The shear-thinning behavior appeared at 4 % w/w. According to the high particle dispersion and the low C_m value (6.4%), the shear-thinning behavior probably resulted from the orientation of the layers under flow. At 6.4%, the occupancy of the Na-smectite layers was such that the entire volume was

occupied, i.e. C_m was reached. These results were in accordance with the detection of a yield stress and a thixotropic behavior.

For the Ca-smectite dispersions, we detected some large entities in dispersion (laser granulometry, Wet STEM) in accordance with the bibliography. Wet STEM images showed large multilayer units (0.07 to 0.77 µm² equivalent ellipse surface). Layers were aggregated in punctual units assuming some attractive interactions. The unit size was highly influenced by the preparation process (laser granulometry). Viscosities of the Ca-smectite dispersions were very low due to the low occupancy of the units. The Ca-smectite dispersion behavior looked like granular dispersion behavior, assuming no or few colloidal interactions. The ϕ_m fm value (0.61) was comparable to ϕ_m of glass ball. However, we recorded a shear-thinning flow for the Ca-smectite dispersions at concentrations higher than 3%. This concentration was strongly below the C_m (11.9%) and the viscosity at rest was very low. Consequently, the shear-thinning behavior could not be explained by the layer orientation due to the occupancy. In the same way, no thixotropic behavior was observed, so no disruption of units occurred. The shear-thinning behavior originated from the deformation of the units under shear stress.

These comparison results between Ca-smectite and Na-smectite seem to be in accordance with the bibliographic values. However, the material can not be considered as a model material due to its natural origin. As each bentonite is singular; the mechanical behavior of the extracted material may change with the modification of one of the preliminary processes (extraction, saturation, dispersion, and preparation). Some heterogeneity in the initial material can affect the reproducibility of these observations with other materials:

- the incomplete extraction of the non-smectitic minerals,
- the type of the dioctahedral smectite (beidellite or montmorillonite), the material used may be a mix of both types,
- the incomplete saturation, and
- the likely formation of sequioxydes during dialysis.

These heterogeneities have no impact on our results because our samples originate from the same material, so they all have the same heterogeneities.

CONLUSION

This study provided adapted extraction and saturation processes to produce smectite in huge quantity. The successive purification steps were adjusted according to the type of raw material and each step was controlled by physicochemical measurements to obtain a large amount of material (800 g). These controlled samples were studied with various methods that were crosschecked and modeled in order to evaluate the structuration of the suspended units according to the saturating cation.

The results showed that the Na-smectite dispersions contained small and thin suspended units that could not be disrupted with the preparation processes used. The Na-smectite units ranges from 0.03 µm² to 0.31 µm², with their shape factor being 50. These widespread entities occupied a large place, which led to a high viscosity at low concentrations. The shear-thinning behavior originated in the orientation of the layers under stress. At rest, without yield stress, the entire volume was occupied at 6.4 %, corresponding to the occurrence of a yield stress.

The Ca-smectite dispersions were composed of several layers linked into large and deformable aggregates. The unit size exhibited a large range of granulometry from 0.07 µm² to 0.77 µm², with their shape factor being 3.3. The dispersions had a low viscosity but a shear-thinning behavior was detected at low concentrations (3 %), which originated from the deformation of the units under shear stress. The maximum volume fraction should be reached at 11.9 %, which corresponds to the apparition of a yield stress.

ACKNOWLEDGMENT

The authors acknowledge A. Bogner and G. Thollet from INSA of Villeurbanne (UMR CNRS 5510) for the Wet STEM use and the Poitou-Charente region for financial support.

REFERENCES

[1] H-H. Murray, Applied Clay Mineralogy, Elsevier, Developments in Clay Science 2, 2007.

[2] F. Bergaya, B.K.G. Theng, G. Lagaly . Handbook of clay science, Elsevier, Developments in Clay Science 1, 2006.

[3] L. Murdoch, D. Wilson, Alternative Methods for Fluid Delivery and Recovery, DIANE Publishing, 1995

[4] T. Permien, G. Lagaly, Clays and Clay Minerals 43 (1995) 229.

[5] G. Lagaly, M. Reese, S. Abend, Applied Clay Science 14 (1999) 83.

[6] P. Coussot. Rhéologie des boues et laves torrentielles, Coll. Etudes du Cemagref, Montagne n°5. Cemagref, Anthony, 1992.

[7] D. Derjaguin, L. Landau, Acta Physicochimica URSS 14 (1941) 633.

[8] E.J.W Verwey, J.T.G. Overbeek. Theory of the stability of lyophobic colloids. Elsevier, Amsterdam, 1948.

[9] J. Lyklema. Fundamentals of Interface and Colloid Science, Volume II, Academic Press, London, 1995.

[10] H. Van Olphen. An introduction to clay colloid chemistry, Wiley, New York, 1977.

[11] O. Touret, C.H. Pons , D. Tessier, Y. Tardy, Clays Minerals 25 (1990) 217.

[12] I. Shainberg, A. Caiserman, Soil Science 111 (1971) 276.

[13] H.A. Velasco-Molina, A.R. Swoboda, C.L. Godfrey, Soil Science 111 (1971) 282.

[14] H. Frenkel, J.O. Goertzen, J.D. Rhoades, Soil Science Society of America Journal 42 (1978) 32.

[15] J.D. Oster, I. Shainberg, J.D. Wood, Soil Science Society of America Journal 44 (1980) 955.

[16] L.L. Schramm, J.C.T. Kwak, Clays Clay Minerals 30 (1982) 40.14

[17] R. Keren, Soil Science Society of America Journal 52 (1988) 924.

[18] W.R. Whalley, C.E. Mullins, Clay Minerals 26 (1991) 11.

[19] C. Malfoy, A. Pantet, P. Monnet, D. Righi, Clays and Clay Minerals 51 (2003) 656.

[20] R. Keren Soil Science Society of America Journal 53 (1989) 25.

[21] H. Zhao, P.F. Low, J.M. Bradford, Soil Science 151 (1991) 196.

[22] K. Verburg, P. Baveye, Clays and Clay Minerals 42 (1994) 207.

[23] R.G. De Kretser, P.J. Scales, D.V. Boger, Colloids and Surfaces A: Physicochemical and Engineering Aspects 137 (1998) 307.

[24] H. Heller, R. Keren, Clays and Clay Minerals 49 (2001) 286.

[25] D. Penner, G. Lagaly, Applied Clay Science 19 (2001) 131.

[26] J.R.V. Pils, D.A. Laird, V.P. Evangelou, Applied Clay Science 35 (2007) 201.

[27] N. Güven, R.M. Pollastro, Clay-water interface and its rheological implications (Güven and R.M. Pollastro editors). CMS Workshop lectures 4, Clay Mineral Society. Boulder, CO., 1992.

[28] G. Lagaly, S. Ziesmer, Colloid and Interface Science 100 (2003) 105.

[29] R.T. Shanmuganathan, J.M. Oades, Geoderma 29 (1983) 257.

[30] A.V. Blackmore, R.D. Miller, Soil Science Society of American Procedure 24 (1961) 169.

[31] I. Shainberg, H. Otoh, Israel Journal of Chemistry 6 (1968) 251.

[32] K. Norrish, J.P. Quirk, Nature 173 (1997) 255.

[33] J. Mewis, Journal of Non-Newtonian Fluids Mechanics 6 (1979) 1.

[34] H.A. Barnes, Journal of Non-Newtonian Fluids Mechanics 70 (1997) 1.

[35] A. Mujumbar, A. Beris, A. Metzner, Journal of Non-Newtonian Fluids Mechanics 2072 (2005) 1.

[36] D.C.H. Cheng, Rheologica Acta, 25 (1986) 542.

[37] J. Schurz, Rheologica Acta 29 (1990) 170.

[38] H.A. Barnes, Journal of Non-Newtonian Fluids Mechanics 81 (1999) 133.

[39] G. Picard, Hétérogénéités de l'écoulement de fluides à seuil : approche phénoménologique et modélisation élasto-plastique. PhD Thesis, University of Paris VII, 2004.

[40] T.F. Tadros Advances in Colloid and Interface Science 68 (1996) 97

[41] H.A. Barnes, Bubbles, Drops and Particles in Non-Newtonian Fluids Mechanics, R.P. Chhabra, CRC Press, Boca Raton FL, 1995.

[42] J. Drappier. Plateaux de contrainte et bandes de cisaillement dans les fluids complexes. PhD Thesis, ENS LPS, university of Paris VII, 2004.

[43] P. Coussot, Rheometry of pastes, suspensions, and granular materials. Applications in industry and environment, Wiley, 1992.

[44] M. Janek, G. Lagaly, Applied Clay Science 19 (2001) 121.

[45] Y. Xiang, G. Villemure, C. Detellier, Clays and Clay Minerals 40 (1992) 362.

[46] D. Fauchadour, T. Pouget, J.P. Lechaire, L. Rouleau, L. Normand, Oil&Gas Science and Technology. Rev. IFP 54 (1999) 513.

[47] G.W. Brindley, G. Brown (eds.), Cristal structures of clay minerals and their X-Ray identification, Monograph 5, Mineralogical society, London, 1980.

[48] A. Bogner, G. Thollet, D. Basset, P.H. Jouneau, C. Gauthier, Ultramicroscopy 104 (2005) 290.

[49] F. Pignon, A. Magnin, J.M. Piau, Journal of Rheology 40 (1996) 573.

[50] P.H.T. Uhlherr, J. Guo, C. Tiu, X.M. Zhang, J.Z.Q. Zhou, T.N. Fang, Journal of Non-Newtonian Fluid Mechanic 125 (2005) 101.

[51] P. Coussot, Mudflow Rheology and Dynamics (A.A. Balkema editor). IAHR Monograph, Rotterdam, 1997.

[52] S. Jarny, N. Roussel, S. Rodts, R. Le Roy, P. Coussot, Concrete Cement Research 35 (2005) 1873.

[53] R.A. Fisher Design of Experiments, Oliver and Boy, Edinburgh, 1935.

[54] G. Tagushi, System of experimental design, Unipub/Kraus International Publication, White Plains, New York, 1987.

[55] P. Coussot, H. Van Damme, in : B. Ildefonse, C. Allain, P. Coussot, Des grands écoulements naturels à la dynamique du tas de sable. Introduction aux suspensions en géologie et en physique, Cemagref, Anthony, 1997.

[56] M. Pawlick, J.S. Laskowski, A. Ansari, Journal of Colloidal and Interface Science 260 (2003) 251.

[57] Y. Peysson, Revue IFP 59 (2004) 11.

[58] R.C. Mackenzie, Differential thermal analysis. Academic press, London and New York, 1970.

[59] A. Cadene, S. Durand-Vidal, P. Turq, J. Brendle, Journal of Colloid and Interface Science 285 (2005) 719.

[60] A. Besq, C. Malfoy, A. Pantet, P. Monnet, D. Righi, Applied Clay Science 23 (2003) 275.

[61] W. Kuhn, H. Kuhn, Helvetica Chimica Acta 28 (1945) 97.

[62] D. Quemada, Modélisation rhéologique structurelle. Dispersions concentrées et fluides complexes. Lavoisier ed., Paris, 2006.

[63] V. N. Kislenko, R. M.Verlinskaya, Journal of Colloid and Interface Science 244 (2001) 405.

Figure 1: Mineralogical evolution of clay during the extraction process: X-Ray Diffractogram of oriented preparations (from 3 to 33 °2θ) of the fine fraction extracted on the 1st, 4th, 8th and 12th extraction cycles. Curves were spaced for more clarity from 10 to 33 °2θ.

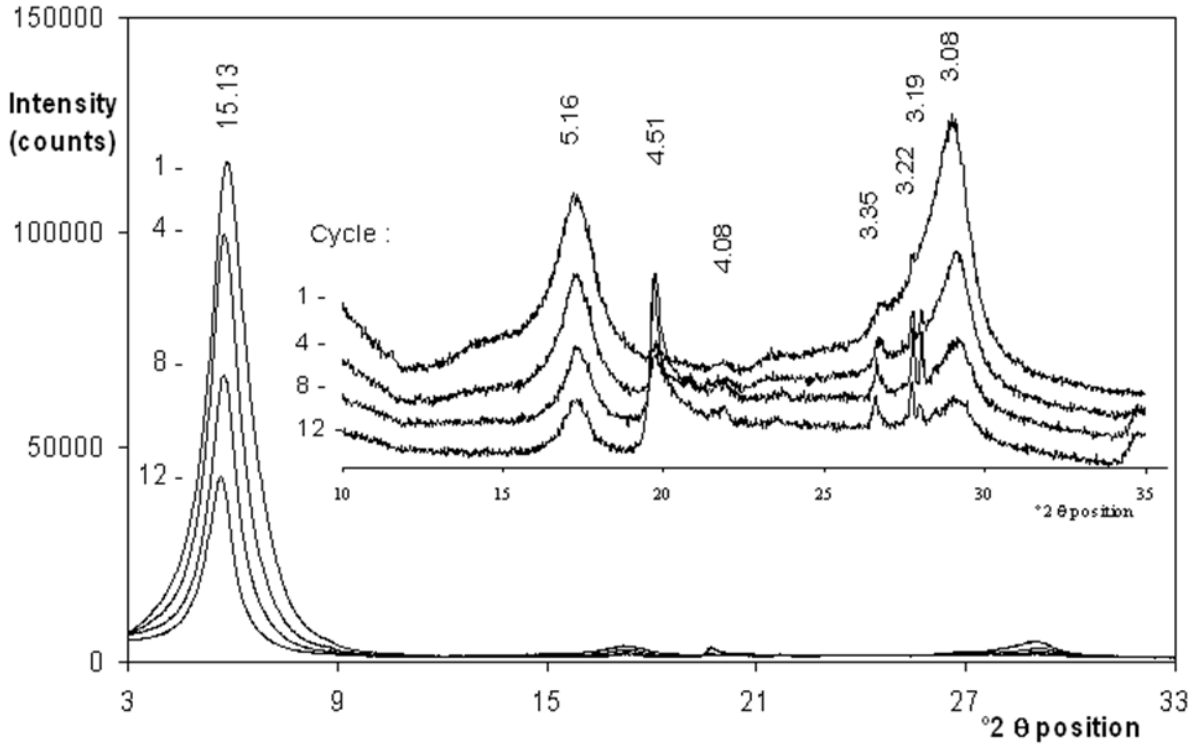

Figure 2: Granulometric evolution of the clay particles during the extraction process: laser granulometry of the fine fraction extracted on the 1st, 4th, 8th and 12th cycles.

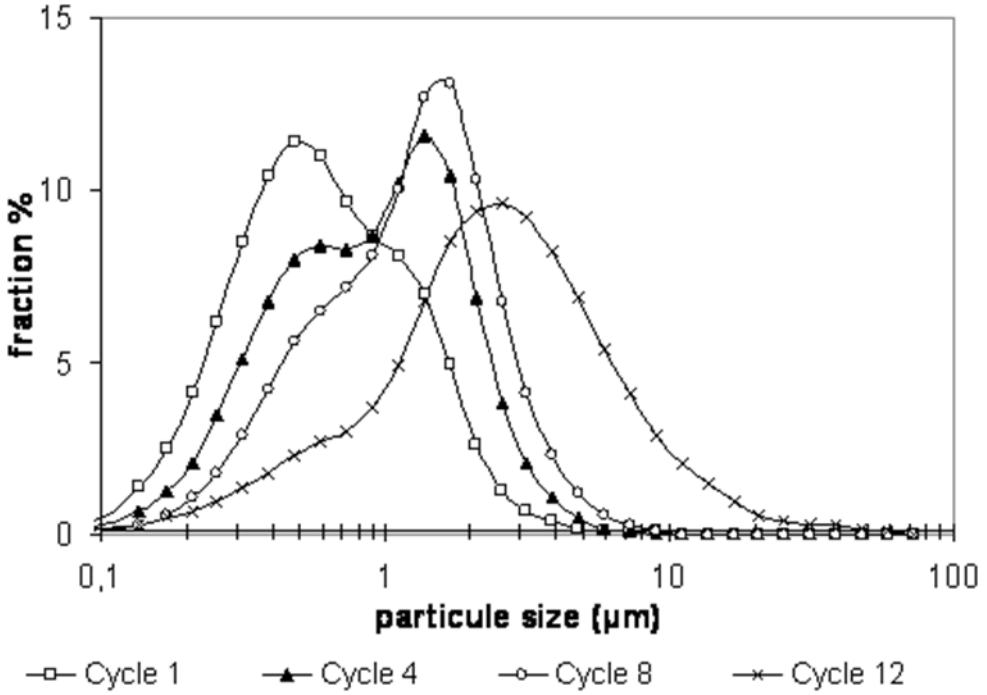

Figure 3: Powder X-ray diffraction patterns of the raw bentonite (upper diffractogram) and the fine fraction (lower diffractogram). They revealed smectite (bold values), quartz (4.260 Å, 3.350 Å), anorthite (3.224 Å, 1.542 Å), opal CT (4.069 Å), mica (3.651 Å) and magnetite (2.520 Å). Curves were spaced for more clarity. Diffractogram intensities ranged from 472 to 16668 counts for raw bentonite and from 579 to 14144 counts for the fine fraction.

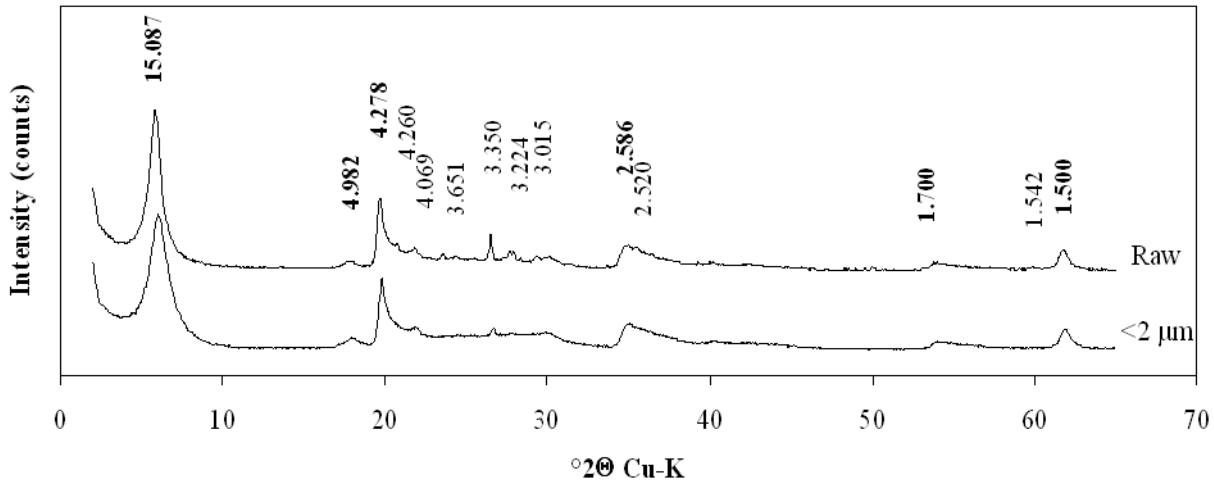

Figure 4: Differential thermal analysis of Ca-smectite and Na-smectite (mass difference between sample and reference as a function of temperature).

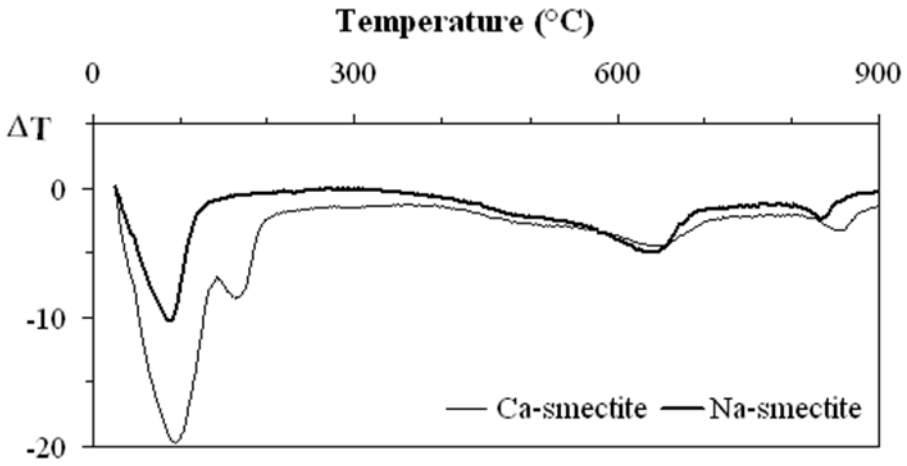

Figure 5: XRD of Ca-smectite and Na-smectite oriented preparations. Where I_{001} is the maximum peak intensity, the d value is the spacing of the lattice plane, B the crystal thickness deduced from the angular width at half-maximum intensity (L), and N the number of layers.

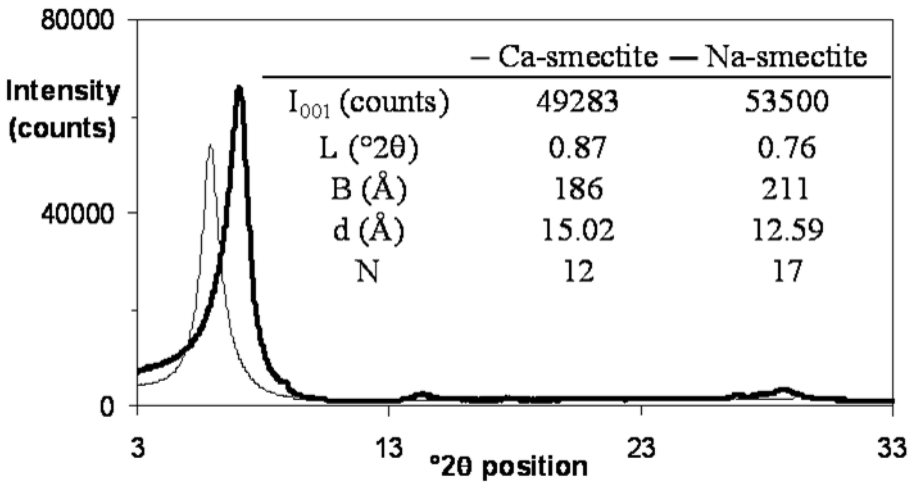

Figure 6: Unit size distribution (laser granulometry) for each sample according to three preparation processes described in (a): hydration process (b), reference process (c) and standard process (d). The index of each curve was presented in (e)

a

Hydration	Reference	Standard
	1*min*	defloculent
	homogenizer	1*min* sonification
10*h* hydration at 50*rpm*		
14*h* hydration		

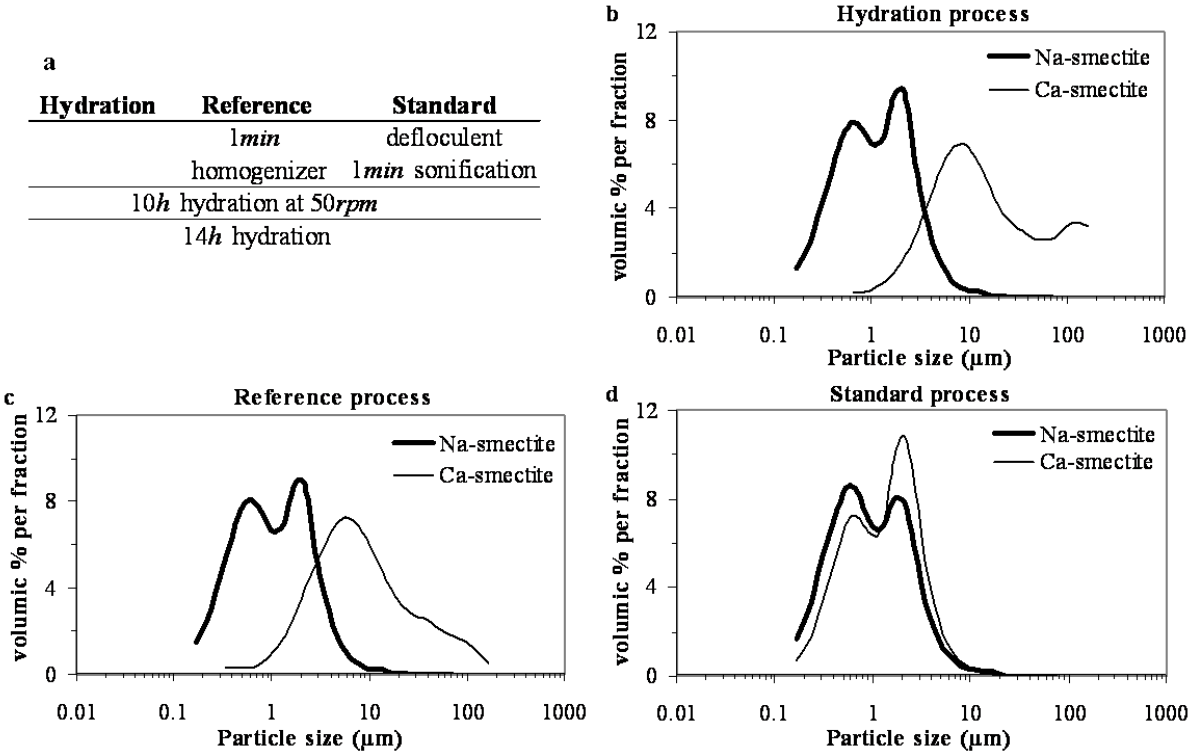

e

Process :	Hydration process		Reference process		Standard process	
Sample :	*Na-smectite*	*Ca-smectite*	*Na-smectite*	*Ca-smectite*	*Na-smectite*	*Ca-smectite*
d_{10} (µm) :	0.3	2.9	0.3	1.9	0.3	0.4
d_{50} (µm) :	1.0	10.6	1.0	7.2	0.8	1.3
d_{90} (µm) :	3.0	106.0	3.0	51.8	3.0	3.7

Figure 7: Wet STEM photographs of Ca-smectite (a : x12,000) and Na-smectite (b : x12,000), photo A. Bogner, INSA Lyon, France. Distribution of the amount of grains according to the particle area (approximate to an ellipse) measured by image processing (c).

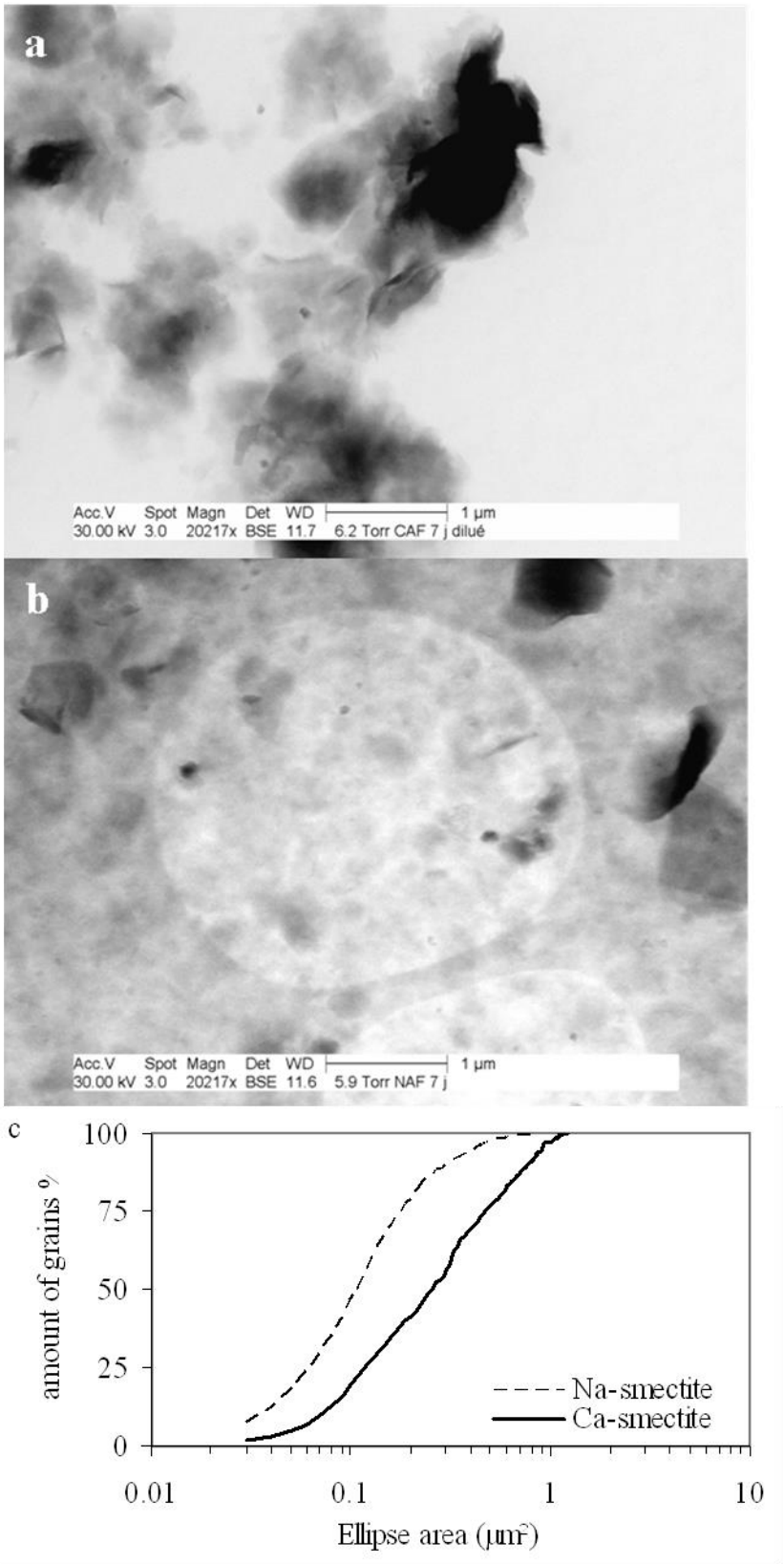

Figure 8: Rheograms for Na-smectite (a) and Ca-smectite (b) at four concentrations (0.2 %, 2 %, 3 %, and 4%).

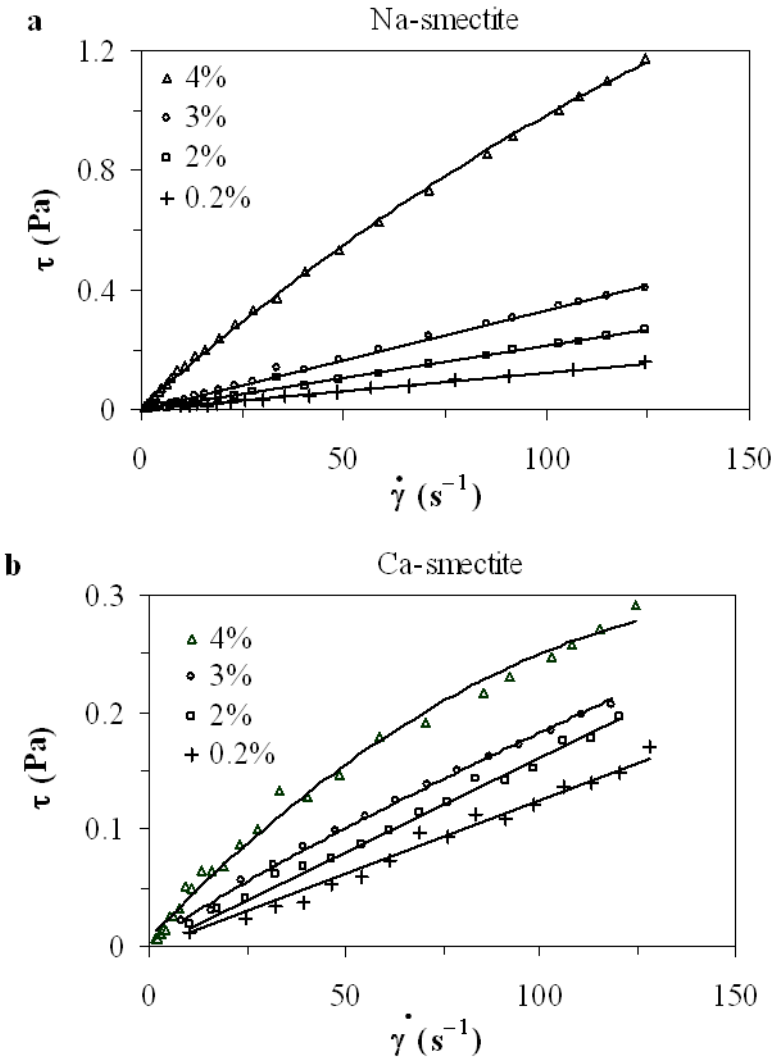

Figure 9: Representation of the relative viscosity against concentration for each sample and modeling with the Krieger-Dougherty law.

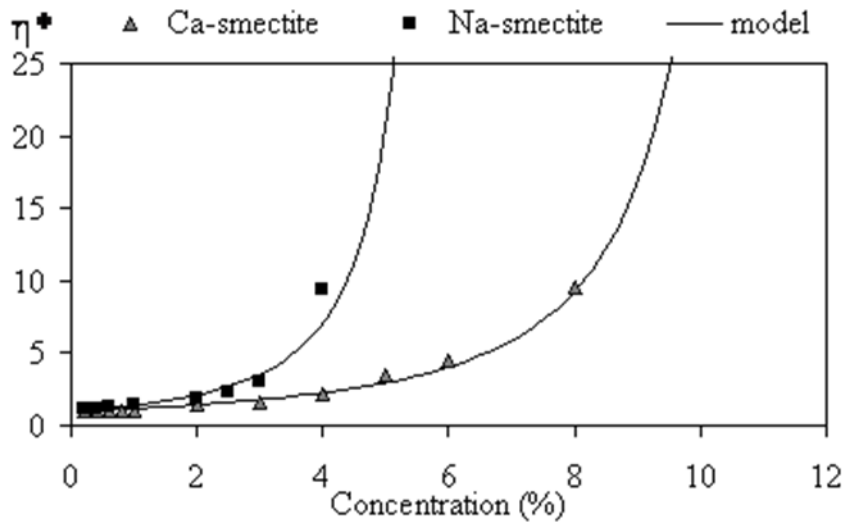

Figure 10: A factor determination according to the Krieger-Dougherty law for Na-smectite and Ca-smectite.

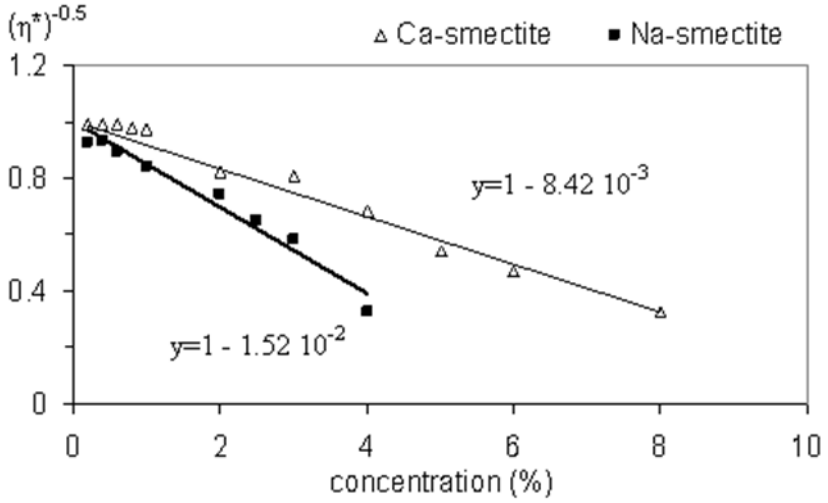

Table 1: Exchangeable cation measurements and CEC of the fine fraction after extraction (*ff*), and after application of the standard and optimized saturation processes (with $CaCl_2$ or NaCl).

	$[Ca^{2+}]$ meq.100g^{-1}	$[Mg^{2+}]$ meq.100g^{-1}	$[K^+]$ meq.100g^{-1}	$[Na^+]$ meq.100g^{-1}	Σ (cations) meq.100g^{-1}	CEC_{NH4} meq.100g^{-1}
Raw fine fraction						
ff	55.6 ± 2.6	33.4 ± 2.4	1.6 ± 0.7	17.1 ± 7.8	107.7 ± 3.7	96 ± 2
Standard saturating process						
with $CaCl_2$	84.5	11.7	2.9	0.0	95.5	95 ± 4
with NaCl	66.3	13.2	3.8	13.4	83.9	84 ± 4
Optimized saturating process						
Ca-smectite	105.4 ± 7.5	4.7 ± 0.0	2.4 ± 0.2	1.6 ± 0.8	114.2 ± 6.2	102 ±5
Na-smectite	1.5 ± 0.6	5.3 ± 0.9	0.1 ± 2	94.3 ± 3.9	101.5 ± 2.3	99 ± 6

Table 2: Chemical analyses of filtrates at 30 % of raw bentonite in water with various delay times (3 hours, one day, one month or 3 months).

Delay	pH	Conductivity µS	F^- mg.l^{-1}	Cl^- mg.l^{-1}	NO_3^- mg.l^{-1}	SO_4^{2-} mg.l^{-1}	Ca^{2+} mg.l^{-1}	Mg^{2+} mg.l^{-1}	Na^+ mg.l^{-1}	K^+ mg.l^{-1}	Σ Cations	Σ Anions
no	8	317	1.4	60.9	0.9	26.5	1.8	1.1	75.6	2.9	81.5	89.7
3 hours	8.1	400	1.7	87.8	1.4	34.9	2.5	1.8	96.0	5.9	106.3	125.8
a day	8.1	478	2.0	98.1	1.5	43.9	4.0	2.6	113.0	9.0	128.6	145.5
a month	8.2	512	1.6	90.6	2.6	46.6	5.2	3.5	118.8	2.5	130.0	141.4
3 months	8.4	556	1.0	110.8	2.2	55.2	7.5	4.6	137.1	3.8	153.0	169.2

Table 3: Oxide percents of the main chemical elements measured with an EDS and deduced structural formula for the fine fraction.

EDS	SiO_2	TiO_2	Al_2O_3	Fe_2O_3	MnO	MgO	CaO	Na_2O	K_2O	$P.F._{1000°C}$	Charge
fine fraction	59.37	0.3	17.69	3.86	0.08	4.85	1.12	0.81	0.5	11.42	0,33

$$(Si_{3.91}Al_{0.03})(Al_{1.37}Ti_{0.01}Fe_{0.19}Mn_{0.01}Mg_{0.38})O_{10}(OH)_2(Ca_{0.08}Na_{0.11}Mg_{0.10}K_{0.04})$$

Table 4: Evolution of the rheological behavior and associated viscosity (η) for each sample according to the concentration.

	Newtonian	Shear thinning	
		no yield	*yield stress*
Na-smectite			
Concentration (% w/w)	4		6
Viscosity η (Pa.s)	$9.9x10^{-3}$		
Ca-smectite			
Concentration (% w/w)	3		11
Viscosity η (Pa.s)	$1.8x10^{-3}$		